

**Search for Neutral Supersymmetric Higgs Bosons
in $p\bar{p}$ Collisions at $\sqrt{s} = 1.8$ TeV**

The CDF Collaboration

Abstract

We present the results of a search for neutral Higgs bosons produced in association with b quarks in $p\bar{p} \rightarrow b\bar{b}\varphi \rightarrow b\bar{b}b\bar{b}$ final states with 91 ± 7 pb⁻¹ of $p\bar{p}$ collisions at $\sqrt{s} = 1.8$ TeV recorded by the Collider Detector at Fermilab. We find no evidence of such a signal and the data is interpreted in the context of the neutral Higgs sector of the Minimal Supersymmetric extension of the Standard Model. With basic parameter choices for the supersymmetric scale and the stop quark mixing, we derive 95% C.L. lower mass limits for neutral Higgs bosons for $\tan\beta$ values in excess of 35.

PACS numbers: 13.85.Rm, 12.15.Ji, 14.80.Bn, 14.80.Cp

Typeset using REVTeX

T. Affolder,²³ H. Akimoto,⁴⁵ A. Akopian,³⁸ M. G. Albrow,¹¹ P. Amaral,⁸ S. R. Amendolia,³⁴ D. Amidei,²⁶ K. Anikeev,²⁴ J. Antos,¹ G. Apollinari,¹¹ T. Arisawa,⁴⁵ T. Asakawa,⁴³ W. Ashmanskas,⁸ F. Azfar,³¹ P. Azzi-Bacchetta,³² N. Bacchetta,³² M. W. Bailey,²⁸ S. Bailey,¹⁶ P. de Barbaro,³⁷ A. Barbaro-Galtieri,²³ V. E. Barnes,³⁶ B. A. Barnett,¹⁹ S. Baroiant,⁵ M. Barone,¹³ G. Bauer,²⁴ F. Bedeschi,³⁴ S. Belforte,⁴² W. H. Bell,¹⁵ G. Bellettini,³⁴ J. Bellinger,⁴⁶ D. Benjamin,¹⁰ J. Bensinger,⁴ A. Beretvas,¹¹ J. P. Berge,¹¹ J. Berryhill,⁸ B. Bevensee,³³ A. Bhatti,³⁸ M. Binkley,¹¹ D. Bisello,³² M. Bishai,¹¹ R. E. Blair,² C. Blocker,⁴ K. Bloom,²⁶ B. Blumenfeld,¹⁹ S. R. Blusk,³⁷ A. Bocci,³⁴ A. Bodek,³⁷ W. Bokhari,³³ G. Bolla,³⁶ Y. Bonushkin,⁶ D. Bortoletto,³⁶ J. Boudreau,³⁵ A. Brandl,²⁸ S. van den Brink,¹⁹ C. Bromberg,²⁷ M. Brozovic,¹⁰ N. Bruner,²⁸ E. Buckley-Geer,¹¹ J. Budagov,⁹ H. S. Budd,³⁷ K. Burkett,¹⁶ G. Busetto,³² A. Byon-Wagner,¹¹ K. L. Byrum,² P. Calafiura,²³ M. Campbell,²⁶ W. Carithers,²³ J. Carlson,²⁶ D. Carlsmith,⁴⁶ W. Caskey,⁵ J. Cassada,³⁷ A. Castro,³² D. Cauz,⁴² A. Cerri,³⁴ A. W. Chan,¹ P. S. Chang,¹ P. T. Chang,¹ J. Chapman,²⁶ C. Chen,³³ Y. C. Chen,¹ M. -T. Cheng,¹ M. Chertok,⁴⁰ G. Chiarelli,³⁴ I. Chirikov-Zorin,⁹ G. Chlachidze,⁹ F. Chlebana,¹¹ L. Christofek,¹⁸ M. L. Chu,¹ Y. S. Chung,³⁷ C. I. Ciobanu,²⁹ A. G. Clark,¹⁴ A. Connolly,²³ J. Conway,³⁹ M. Cordelli,¹³ J. Cranshaw,⁴¹ D. Cronin-Hennessy,¹⁰ R. Cropp,²⁵ R. Culbertson,¹¹ D. Dagenhart,⁴⁴ S. D'Auria,¹⁵ F. DeJongh,¹¹ S. Dell'Agnello,¹³ M. Dell'Orso,³⁴ L. Demortier,³⁸ M. Deninno,³ P. F. Derwent,¹¹ T. Devlin,³⁹ J. R. Dittmann,¹¹ S. Donati,³⁴ J. Done,⁴⁰ T. Dorigo,¹⁶ N. Eddy,¹⁸ K. Einsweiler,²³ J. E. Elias,¹¹ E. Engels, Jr.,³⁵ D. Errede,¹⁸ S. Errede,¹⁸ Q. Fan,³⁷ R. G. Feild,⁴⁷ J. P. Fernandez,¹¹ C. Ferretti,³⁴ R. D. Field,¹² I. Fiori,³ B. Flaughner,¹¹ G. W. Foster,¹¹ M. Franklin,¹⁶ J. Freeman,¹¹ J. Friedman,²⁴ Y. Fukui,²² I. Furic,²⁴ S. Galeotti,³⁴ M. Gallinaro,³⁸ T. Gao,³³ M. Garcia-Sciveres,²³ A. F. Garfinkel,³⁶ P. Gatti,³² C. Gay,⁴⁷ D. W. Gerdes,²⁶ P. Giannetti,³⁴ P. Giromini,¹³ V. Glagolev,⁹ M. Gold,²⁸ J. Goldstein,¹¹ A. Gordon,¹⁶ I. Gorelov,²⁸ A. T. Goshaw,¹⁰ Y. Gotra,³⁵ K. Goulianos,³⁸ C. Green,³⁶ G. Grim,⁵ P. Gris,¹¹ L. Groer,³⁹ C. Grosso-Pilcher,⁸ M. Guenther,³⁶ G. Guillian,²⁶ J. Guimaraes da Costa,¹⁶ R. M. Haas,¹² C. Haber,²³ E. Hafen,²⁴ S. R. Hahn,¹¹ C. Hall,¹⁶

T. Handa,¹⁷ R. Handler,⁴⁶ W. Hao,⁴¹ F. Happacher,¹³ K. Hara,⁴³ A. D. Hardman,³⁶
 R. M. Harris,¹¹ F. Hartmann,²⁰ K. Hatakeyama,³⁸ J. Hauser,⁶ J. Heinrich,³³ A. Heiss,²⁰
 M. Herndon,¹⁹ C. Hill,⁵ K. D. Hoffman,³⁶ C. Holck,³³ R. Hollebeek,³³ L. Holloway,¹⁸
 R. Hughes,²⁹ J. Huston,²⁷ J. Huth,¹⁶ H. Ikeda,⁴³ J. Incandela,¹¹ G. Introzzi,³⁴ J. Iwai,⁴⁵
 Y. Iwata,¹⁷ E. James,²⁶ H. Jensen,¹¹ M. Jones,³³ U. Joshi,¹¹ H. Kambara,¹⁴ T. Kamon,⁴⁰
 T. Kaneko,⁴³ K. Karr,⁴⁴ H. Kasha,⁴⁷ Y. Kato,³⁰ T. A. Keaffaber,³⁶ K. Kelley,²⁴ M. Kelly,²⁶
 R. D. Kennedy,¹¹ R. Kephart,¹¹ D. Khazins,¹⁰ T. Kikuchi,⁴³ B. Kilminster,³⁷ B. J. Kim,²¹
 D. H. Kim,²¹ H. S. Kim,¹⁸ M. J. Kim,²¹ S. H. Kim,⁴³ Y. K. Kim,²³ M. Kirby,¹⁰ M. Kirk,⁴
 L. Kirsch,⁴ S. Klimenko,¹² P. Koehn,²⁹ A. Köngeter,²⁰ K. Kondo,⁴⁵ J. Konigsberg,¹²
 K. Kordas,²⁵ A. Korn,²⁴ A. Korytov,¹² E. Kovacs,² J. Kroll,³³ M. Kruse,³⁷ S. E. Kuhlmann,²
 K. Kurino,¹⁷ T. Kuwabara,⁴³ A. T. Laasanen,³⁶ N. Lai,⁸ S. Lami,³⁸ S. Lammel,¹¹
 J. I. Lamoureux,⁴ J. Lancaster,¹⁰ M. Lancaster,²³ R. Lander,⁵ G. Latino,³⁴ T. LeCompte,²
 A. M. Lee IV,¹⁰ K. Lee,⁴¹ S. Leone,³⁴ J. D. Lewis,¹¹ M. Lindgren,⁶ T. M. Liss,¹⁸ J. B. Liu,³⁷
 Y. C. Liu,¹ N. Lockyer,³³ J. Loken,³¹ M. Loretì,³² D. Lucchesi,³² P. Lukens,¹¹ S. Lusin,⁴⁶
 L. Lyons,³¹ J. Lys,²³ R. Madrak,¹⁶ K. Maeshima,¹¹ P. Maksimovic,¹⁶ L. Malferrari,³
 M. Mangano,³⁴ M. Mariotti,³² G. Martignon,³² A. Martin,⁴⁷ J. A. J. Matthews,²⁸ J. Mayer,²⁵
 P. Mazzanti,³ K. S. McFarland,³⁷ P. McIntyre,⁴⁰ E. McKigney,³³ M. Menguzzato,³²
 A. Menzione,³⁴ C. Mesropian,³⁸ A. Meyer,¹¹ T. Miao,¹¹ R. Miller,²⁷ J. S. Miller,²⁶
 H. Minato,⁴³ S. Miscetti,¹³ M. Mishina,²² G. Mitselmakher,¹² N. Moggi,³ E. Moore,²⁸
 R. Moore,²⁶ Y. Morita,²² M. Mulhearn,²⁴ A. Mukherjee,¹¹ T. Muller,²⁰ A. Munar,³⁴
 P. Murat,¹¹ S. Murgia,²⁷ J. Nachtman,⁶ S. Nahn,⁴⁷ H. Nakada,⁴³ T. Nakaya,⁸ I. Nakano,¹⁷
 C. Nelson,¹¹ T. Nelson,¹¹ C. Neu,²⁹ D. Neuberger,²⁰ C. Newman-Holmes,¹¹ C.-Y. P. Ngan,²⁴
 H. Niu,⁴ L. Nodulman,² A. Nomerotski,¹² S. H. Oh,¹⁰ T. Ohmoto,¹⁷ T. Ohsugi,¹⁷
 R. Oishi,⁴³ T. Okusawa,³⁰ J. Olsen,⁴⁶ W. Orejudos,²³ C. Pagliarone,³⁴ F. Palmonari,³⁴
 R. Paoletti,³⁴ V. Papadimitriou,⁴¹ S. P. Pappas,⁴⁷ D. Partos,⁴ J. Patrick,¹¹ G. Pauletta,⁴²
 M. Paulini,^{(*) 23} C. Paus,²⁴ L. Pescara,³² T. J. Phillips,¹⁰ G. Piacentino,³⁴ K. T. Pitts,¹⁸
 A. Pompos,³⁶ L. Pondrom,⁴⁶ G. Pope,³⁵ M. Popovic,²⁵ F. Prokoshin,⁹ J. Proudfoot,²
 F. Ptohos,¹³ O. Pukhov,⁹ G. Punzi,³⁴ K. Ragan,²⁵ A. Rakitine,²⁴ D. Reher,²³ A. Reichold,³¹

A. Ribon,³² W. Riegler,¹⁶ F. Rimondi,³ L. Ristori,³⁴ M. Riveline,²⁵ W. J. Robertson,¹⁰
A. Robinson,²⁵ T. Rodrigo,⁷ S. Rolli,⁴⁴ L. Rosenson,²⁴ R. Roser,¹¹ R. Rossin,³² A. Safonov,³⁸
R. St. Denis,¹⁵ W. K. Sakumoto,³⁷ D. Saltzberg,⁶ C. Sanchez,²⁹ A. Sansoni,¹³ L. Santi,⁴²
H. Sato,⁴³ P. Savard,²⁵ P. Schlabach,¹¹ E. E. Schmidt,¹¹ M. P. Schmidt,⁴⁷ M. Schmitt,¹⁶
L. Scodellaro,³² A. Scott,⁶ A. Scribano,³⁴ S. Segler,¹¹ S. Seidel,²⁸ Y. Seiya,⁴³ A. Semenov,⁹
F. Semeria,³ T. Shah,²⁴ M. D. Shapiro,²³ P. F. Shepard,³⁵ T. Shibayama,⁴³ M. Shimojima,⁴³
M. Shochet,⁸ J. Siegrist,²³ G. Signorelli,³⁴ A. Sill,⁴¹ P. Sinervo,²⁵ P. Singh,¹⁸ A. J. Slaughter,⁴⁷
K. Sliwa,⁴⁴ C. Smith,¹⁹ F. D. Snider,¹¹ A. Solodsky,³⁸ J. Spalding,¹¹ T. Speer,¹⁴ P. Sphicas,²⁴
F. Spinella,³⁴ M. Spiropulu,¹⁶ L. Spiegel,¹¹ J. Steele,⁴⁶ A. Stefanini,³⁴ J. Strologas,¹⁸
F. Strumia,¹⁴ D. Stuart,¹¹ K. Sumorok,²⁴ T. Suzuki,⁴³ T. Takano,³⁰ R. Takashima,¹⁷
K. Takikawa,⁴³ P. Tamburello,¹⁰ M. Tanaka,⁴³ B. Tannenbaum,⁶ W. Taylor,²⁵ M. Tecchio,²⁶
P. K. Teng,¹ K. Terashi,³⁸ S. Tether,²⁴ A. S. Thompson,¹⁵ R. Thurman-Keup,² P. Tipton,³⁷
S. Tkaczyk,¹¹ K. Tollefson,³⁷ A. Tollestrup,¹¹ H. Toyoda,³⁰ W. Trischuk,²⁵ J. F. de Troconiz,¹⁶
J. Tseng,²⁴ N. Turini,³⁴ F. Ukegawa,⁴³ T. Vaiciulis,³⁷ J. Valls,³⁹ S. Vejcik III,¹¹ G. Velez,¹¹
R. Vidal,¹¹ R. Vilar,⁷ I. Volobouev,²³ D. Vucinic,²⁴ R. G. Wagner,² R. L. Wagner,¹¹ J. Wahl,⁸
N. B. Wallace,³⁹ A. M. Walsh,³⁹ C. Wang,¹⁰ M. J. Wang,¹ T. Watanabe,⁴³ D. Waters,³¹
T. Watts,³⁹ R. Webb,⁴⁰ H. Wenzel,²⁰ W. C. Wester III,¹¹ A. B. Wicklund,² E. Wicklund,¹¹
T. Wilkes,⁵ H. H. Williams,³³ P. Wilson,¹¹ B. L. Winer,²⁹ D. Winn,²⁶ S. Wolbers,¹¹
D. Wolinski,²⁶ J. Wolinski,²⁷ S. Wolinski,²⁶ S. Worm,²⁸ X. Wu,¹⁴ J. Wyss,³⁴ A. Yagil,¹¹
W. Yao,²³ G. P. Yeh,¹¹ P. Yeh,¹ J. Yoh,¹¹ C. Yosef,²⁷ T. Yoshida,³⁰ I. Yu,²¹ S. Yu,³³ Z. Yu,⁴⁷
A. Zanetti,⁴² F. Zetti,²³ and S. Zucchelli³

(CDF Collaboration)

¹ *Institute of Physics, Academia Sinica, Taipei, Taiwan 11529, Republic of China*

² *Argonne National Laboratory, Argonne, Illinois 60439*

³ *Istituto Nazionale di Fisica Nucleare, University of Bologna, I-40127 Bologna, Italy*

⁴ *Brandeis University, Waltham, Massachusetts 02254*

- ⁵ *University of California at Davis, Davis, California 95616*
- ⁶ *University of California at Los Angeles, Los Angeles, California 90024*
- ⁷ *Instituto de Fisica de Cantabria, CSIC-University of Cantabria, 39005 Santander, Spain*
- ⁸ *Enrico Fermi Institute, University of Chicago, Chicago, Illinois 60637*
- ⁹ *Joint Institute for Nuclear Research, RU-141980 Dubna, Russia*
- ¹⁰ *Duke University, Durham, North Carolina 27708*
- ¹¹ *Fermi National Accelerator Laboratory, Batavia, Illinois 60510*
- ¹² *University of Florida, Gainesville, Florida 32611*
- ¹³ *Laboratori Nazionali di Frascati, Istituto Nazionale di Fisica Nucleare, I-00044 Frascati, Italy*
- ¹⁴ *University of Geneva, CH-1211 Geneva 4, Switzerland*
- ¹⁵ *Glasgow University, Glasgow G12 8QQ, United Kingdom*
- ¹⁶ *Harvard University, Cambridge, Massachusetts 02138*
- ¹⁷ *Hiroshima University, Higashi-Hiroshima 724, Japan*
- ¹⁸ *University of Illinois, Urbana, Illinois 61801*
- ¹⁹ *The Johns Hopkins University, Baltimore, Maryland 21218*
- ²⁰ *Institut für Experimentelle Kernphysik, Universität Karlsruhe, 76128 Karlsruhe, Germany*
- ²¹ *Center for High Energy Physics: Kyungpook National University, Taegu 702-701; Seoul National University, Seoul 151-742; and SungKyunKwan University, Suwon 440-746; Korea*
- ²² *High Energy Accelerator Research Organization (KEK), Tsukuba, Ibaraki 305, Japan*
- ²³ *Ernest Orlando Lawrence Berkeley National Laboratory, Berkeley, California 94720*
- ²⁴ *Massachusetts Institute of Technology, Cambridge, Massachusetts 02139*
- ²⁵ *Institute of Particle Physics: McGill University, Montreal H3A 2T8; and University of Toronto, Toronto M5S 1A7;*
Canada
- ²⁶ *University of Michigan, Ann Arbor, Michigan 48109*
- ²⁷ *Michigan State University, East Lansing, Michigan 48824*
- ²⁸ *University of New Mexico, Albuquerque, New Mexico 87131*
- ²⁹ *The Ohio State University, Columbus, Ohio 43210*
- ³⁰ *Osaka City University, Osaka 588, Japan*

- ³¹ *University of Oxford, Oxford OX1 3RH, United Kingdom*
- ³² *Universita di Padova, Istituto Nazionale di Fisica Nucleare, Sezione di Padova, I-35131 Padova, Italy*
- ³³ *University of Pennsylvania, Philadelphia, Pennsylvania 19104*
- ³⁴ *Istituto Nazionale di Fisica Nucleare, University and Scuola Normale Superiore of Pisa, I-56100 Pisa, Italy*
- ³⁵ *University of Pittsburgh, Pittsburgh, Pennsylvania 15260*
- ³⁶ *Purdue University, West Lafayette, Indiana 47907*
- ³⁷ *University of Rochester, Rochester, New York 14627*
- ³⁸ *Rockefeller University, New York, New York 10021*
- ³⁹ *Rutgers University, Piscataway, New Jersey 08855*
- ⁴⁰ *Texas A&M University, College Station, Texas 77843*
- ⁴¹ *Texas Tech University, Lubbock, Texas 79409*
- ⁴² *Istituto Nazionale di Fisica Nucleare, University of Trieste/ Udine, Italy*
- ⁴³ *University of Tsukuba, Tsukuba, Ibaraki 305, Japan*
- ⁴⁴ *Tufts University, Medford, Massachusetts 02155*
- ⁴⁵ *Waseda University, Tokyo 169, Japan*
- ⁴⁶ *University of Wisconsin, Madison, Wisconsin 53706*
- ⁴⁷ *Yale University, New Haven, Connecticut 06520*
- (*) *Now at Carnegie Mellon University, Pittsburgh, Pennsylvania 15213*

A fundamental question which remains open today in particle physics is the origin of the electroweak symmetry breaking. The simplest mechanism in the Standard Model (SM) and in many supersymmetric extensions is spontaneous symmetry breaking, achieved through the introduction of one or more scalar field doublets. The SM assumes one doublet of scalar fields and a single physical Higgs boson (h_{SM}), with unknown mass but with fixed couplings to other particles. A more complex symmetry breaking mechanism occurs in the Minimal Supersymmetric extension of the Standard Model (MSSM), where several physical scalar states are predicted: three neutral bosons (the CP-even h and H , and the CP-odd A) and two charged bosons (H^\pm). A distinct feature of the MSSM is the modified couplings of the Higgs particles, in particular the enhancement of the bottom-Higgs Yukawa couplings by $\tan\beta$ for the case of the bbA vertex, where $\tan\beta$ is the ratio of the vacuum expectation values of the two Higgs doublets of the theory. The Higgs sector of the MSSM is completely determined at tree level by two free parameters, chosen to be the mass of the CP-odd Higgs boson, m_A , and $\tan\beta$. The mass of the CP-even Higgs boson h , m_h , is constrained to be less than $m_{Z^0}|\cos 2\beta|$. Radiative corrections substantially modify the masses and couplings of the two neutral CP-even Higgs scalars, in particular the upper bound on m_h [1].

At the Tevatron, one of the Higgs production mechanisms likely to be observed in both the SM and some regions of the MSSM parameter space is the associated production $p\bar{p} \rightarrow V + \varphi$, where $V = W, Z$ and $\varphi = h, H, h_{SM}$. CDF has already reported on searches for this channel ($V + h_{SM}$) with different signatures [2,3]. In this Letter we exploit the enhanced bottom-Higgs Yukawa couplings of the MSSM to test the large $\tan\beta$ sector of the theory by searching for the process $p\bar{p} \rightarrow b\bar{b}\varphi \rightarrow b\bar{b}b\bar{b}$ with $\varphi = h, H, A$. Our sensitivity in this search is limited to the region of parameter space corresponding to $\tan\beta \gtrsim 35$. In this region, at least one of the CP-even Higgs bosons has similar couplings to, and is always degenerate with, the CP-odd Higgs boson. For $m_A \lesssim 110 - 125 \text{ GeV}/c^2$ (depending on $\tan\beta$ and on the parameters of the stop quark mass matrix), $m_h \simeq m_A$, while for $m_A \gtrsim 110 - 125 \text{ GeV}/c^2$, $m_H \simeq m_A$. Therefore this analysis covers a simultaneous search for two or more Higgs

signals with an experimental signature of four b jets in the final state.

The search reported here is based on $91 \pm 7 \text{ pb}^{-1}$ of integrated luminosity recorded during the 1994-95 Tevatron run. The CDF detector is described in detail elsewhere [4]. The silicon vertex detector (SVX) consists of four layers of axial microstrips located immediately outside the beampipe with an innermost radius of 2.9 cm [5]. The SVX provides precise track reconstruction in the plane perpendicular to the beam and the ability to identify secondary vertices produced by heavy flavor decays. The momenta of charged particles are measured in the central tracking chamber (CTC), which lies inside a 1.4 T superconducting solenoidal magnet. Outside the CTC, electromagnetic and hadronic calorimeters arranged in a projective tower geometry cover the pseudorapidity region $|\eta| < 4.2$ [6] and are used to identify jets. The data sample was recorded with a trigger which requires four or more clusters of contiguous calorimeter towers, each with transverse energy $E_T \geq 15 \text{ GeV}$, and a total transverse energy $\sum E_T \geq 125 \text{ GeV}$.

The initial steps of the data selection are the same as in the recent CDF SM Higgs search [3]. We start by rejecting cosmic ray events, beam halo, and detector noise. Events with one or more identified electrons or muons from vector boson decays defined as in [2] are also rejected. After this selection, events are required to have at least four jets with $E_T \geq 15 \text{ GeV}$ and well contained within the fiducial calorimeter regions $|\eta| \leq 1.5$. Jets are defined as localized energy depositions in the calorimeters and are reconstructed using an iterative clustering algorithm with a fixed cone of radius $\Delta R = \sqrt{\Delta\eta^2 + \Delta\phi^2} = 0.4$ in $\eta - \phi$ space [7]. Jet energies are corrected for energy losses in uninstrumented detector regions, energy falling outside the clustering cone, contributions from underlying event and multiple interactions, and calorimeter nonlinearities. The selected data sample is dominated by QCD multijet events and contains 207,604 events. The four highest- E_T jets in an event are then ordered in E_T and a search sample is obtained for each of a set of Higgs boson masses by requiring the three highest- E_T jets to pass cuts which are Higgs boson mass dependent. This is motivated by the fact that the E_T spectrum of the leading jets for the

signal is, on average, larger than the QCD background, and grows with increasing scalar boson mass (m_φ). We use the leading order (LO) parton level matrix elements [8] encoded in the PYTHIA v5.6 Monte Carlo program [9] along with a full simulation of the CDF detector to simulate the signal. We use the CTEQ3L parton distribution functions and set a factorization scale equal to the Higgs boson mass in the simulation. We find optimal E_T cuts by maximizing the expected significance of the signal. For a Higgs boson mass of $m_\varphi = 120 \text{ GeV}/c^2$ these cuts correspond to 48, 34 and 15 GeV for the leading jet, second and third leading jets of the event, respectively, and vary roughly linearly with the Higgs boson mass. We then require that at least three among the four highest- E_T jets in the event are identified (tagged) as b quark candidates. The algorithm used to identify secondary vertices [10] begins by searching for jets which contain three or more displaced tracks. If none are found, the algorithm searches for two-track vertices using more stringent track criteria. A jet is tagged if the transverse displacement of the secondary vertex from the primary vertex exceeds three times its uncertainty. A requirement on the azimuthal angular distribution of the two highest- E_T b -tagged jets in the event, $\Delta\varphi_{b\bar{b}} > 109^\circ$, reduces the heavy flavor QCD content of the sample attributed to gluon splitting. This cut preserves $\sim 90\%$ of the signal events which favor a larger angular separation between the b -tagged jets coming from the Higgs decay. After the three tag requirement and the $\Delta\varphi$ cut we are left with 20 and 13 events, respectively, for the case of the $m_\varphi = 70 \text{ GeV}/c^2$ selection.

To reconstruct the signal we select one of the possible invariant mass combinations between the highest- E_T jets in the event. From Monte Carlo we find that the mass of the highest- E_T jets in the event (m_{12}) for signal masses $m_\varphi > 120 \text{ GeV}/c^2$, and the mass of the second and third highest- E_T jets in the event (m_{23}) for signal masses $m_\varphi \leq 120 \text{ GeV}/c^2$ enhance the signal resolution, $\delta(m_\varphi)/m_\varphi$. The use of these distributions also minimizes the percentage of events for which at least one of the jets in the dijet mass is not associated with a b quark from a Higgs boson decay. All signal mass distributions contain a Gaussian core with a resolution which depends on the Higgs boson mass and varies from $\sim 25\%$ for

$m_\varphi \leq 120 \text{ GeV}/c^2$ to $\sim 13\%$ for $m_\varphi > 120 \text{ GeV}/c^2$. We increase the expected significance of the signal by applying mass window cuts on the m_{12} and m_{23} distributions which vary between $\pm 1\delta(m_\varphi)$ and $\pm 3\delta(m_\varphi)$, depending on the Higgs mass, and centered on the mean of the fit distributions. A cut on the invariant mass distribution between the two b -tagged highest- E_T jets of the event further discriminates against heavy flavor QCD events. All mass cuts were chosen to maximize the expected significance of the signal. Table I shows the number of observed triple b -tagged events left after all cuts as a function of mass. Five events are left after all cuts in the mass bin at $70 \text{ GeV}/c^2$. All events for the mass bins above $70 \text{ GeV}/c^2$ are included in this sample of five events.

In addition to the large QCD multijet background, other sources of heavy flavor in the triple b -tagged sample include multijet $t\bar{t}$ production ($t \rightarrow Wb$, $W \rightarrow q\bar{q}'$), $Wb\bar{b}$ and $Wc\bar{c}$ with $W \rightarrow q\bar{q}'$, $Zb\bar{b}$ and $Zc\bar{c}$ with $Z \rightarrow b\bar{b}/c\bar{c}$, and fake triple-tags. They are estimated from a combination of Monte Carlo and data. We use the HERWIG v5.6 Monte Carlo generator [11] with the CDF measured cross section ($\sigma_{t\bar{t}} = 6.5^{+1.7}_{-1.4} \text{ pb}$) [12] and a top mass of $m_t = 175 \text{ GeV}/c^2$ to predict the expected number of $t\bar{t}$ events. Electroweak processes are also estimated with the same Monte Carlo generator. Fake triple-tags are defined as events in which at least one of the three b -tagged jets contains a false secondary vertex in a light quark or gluon jet. Fake tag probabilities are parameterized by measuring in several inclusive jet data samples the fraction of jets in which a secondary vertex is reconstructed on the wrong side of the primary vertex with respect to the jet direction [10,13].

The same fit technique that was used to estimate the QCD heavy flavor normalization in the SM Higgs search [3] is applied to this analysis. We reduce the b -tag cuts on our data sample from triple to double b -tags. This gives a high statistics background-rich sample in which we fit the double b -tagged dijet mass distribution to a combination of signal and SM backgrounds. The shape of the QCD heavy flavor distribution is obtained from the PYTHIA Monte Carlo program. We generate all QCD jet production channels, and retain the events that contain a heavy quark produced either in the hard scattering or in the

associated radiation process. The signal and QCD normalization is left free in the fit while the SM non-QCD background, both shape and normalization, is obtained from Monte Carlo simulation. The QCD normalization in our triple b -tagged sample is then obtained from the ratio of normalizations of double b -tagged to triple b -tagged QCD events taken from the PYTHIA Monte Carlo simulation. Table II lists the individual QCD, $t\bar{t}$, $Wb\bar{b}$, $Wc\bar{c}$, $Zb\bar{b}$, $Zc\bar{c}$, fake triple tags, and total expected contributions to the final observed sample as a function of mass. From these numbers we find no evidence for the presence of a Higgs boson signal. Figure 1 shows the m_{12} and m_{23} distributions for the observed triple b -tagged sample compared to the SM background expectations and for three different selections corresponding to $m_\varphi = 70, 120, \text{ and } 200 \text{ GeV}/c^2$. Also shown are the signal plus background shapes normalized to the expected number of events for $\tan\beta = 50$ and the case of no mixing in the scalar top sector (*no mixing* scenario).

We calculate the signal detection efficiencies and normalizations from Monte Carlo. The overall detection acceptances with their total uncertainties are shown in Table I as a function of mass. They are within a range of 0.2% to 0.6%, increasing with mass. This low acceptance is dominated by the small multijet trigger efficiencies ($\sim 1\%$ to $\sim 7\%$, increasing with the signal mass) and, to a lesser extent, by the triple b -tag requirement ($\sim 20\%$). The low values for the trigger efficiency are due to the high E_T thresholds and multiplicity requirements on jets. The trigger efficiency curves have been obtained with a trigger simulation with parametrized curves estimated from data. The total systematic error includes uncertainties in the multijet trigger simulation (5%), in the modelling of gluon radiation (10% to 7%, depending on the mass), in the calorimeter energy scale (10% to 2%, depending on the mass), in the luminosity measurement (7%), and in the b -tag efficiencies (10%).

From the data in Table I we set upper limits on $b\bar{b}\varphi \rightarrow b\bar{b}b\bar{b}$ ($\varphi = h, H, A$) production using a one-sided conditional frequentist construction [14], where systematic uncertainties are approximately taken into account by Bayesian averaging over the systematic parameters [15], assuming gaussian a-priori distributions around their best estimates. The 95%

C.L. upper limits on the total expected signal events as well as on the production cross section times branching fraction are listed in Table I. Using the LO theoretical cross sections for $\sigma(p\bar{p} \rightarrow b\bar{b}\varphi)\mathcal{BR}(\varphi \rightarrow b\bar{b})$ with $\varphi = h, H, A$ and the bottom-Higgs Yukawa coupling calculated with a running bottom quark mass evaluated at the Higgs boson mass scale, $m_b(m_\varphi) \simeq 3 \text{ GeV}/c^2$, we exclude regions of parameter space for $m_h - \tan\beta$ and $m_A - \tan\beta$, respectively, as shown in Figures 2 and 3. Results are shown for two common choices of the stop quark mixing parameter [1]: *no mixing* ($A_t = \mu \cot\beta$), and *maximal mixing* ($A_t = \mu \cot\beta + \sqrt{6} m_S$, with μ the supersymmetric Higgs boson mass parameter and A_t a soft breaking parameter). In all cases we set m_S , the supersymmetric mass scale, to be 1 TeV/ c^2 and $m_t = 175 \text{ GeV}/c^2$. As a test of the sensitivity of our calculated limits to the background estimate, if we assume a zero background hypothesis the result limits increase, for all signal masses, by $\delta(\tan\beta) = 10$.

In conclusion, we have searched for neutral Higgs bosons produced in association with b quarks through the reaction $p\bar{p} \rightarrow b\bar{b}\varphi \rightarrow b\bar{b}b\bar{b}$. We do not find evidence for the presence of a signal and 95% C.L. upper limits are set on the production cross section times branching ratio. The results have been interpreted in the context of the MSSM Higgs sector and lower mass limits for neutral Higgs bosons derived for $\tan\beta$ values in excess of 35.

We thank the Fermilab staff and the technical staffs of the participating institutions for their vital contributions. This work was supported by the U.S. Department of Energy, the National Science Foundation, the Istituto Nazionale di Fisica Nucleare (Italy), the Ministry of Science, Culture and Education of Japan, the Natural Sciences and Engineering Council of Canada, the National Science Council of the Republic of China, and the A. P. Sloan Foundation.

REFERENCES

- [1] M. Carena et al., CERN-TH-99-374, hep-ph/9912223.
- [2] F. Abe *et al.*, Phys. Rev. Lett. **79**, 3819 (1997).
- [3] F. Abe *et al.*, Phys. Rev. Lett. **81**, 5748 (1998).
- [4] F. Abe *et al.*, Nucl. Instrum. Methods Phys. Res., Sect. A **271**, 387 (1988).
- [5] D. Amidei *et al.*, Nucl. Instrum. Methods Phys. Res., Sect. A **350**, 73 (1994).
- [6] In the CDF coordinate system, ϕ and θ are the azimuthal and polar angles with respect to the proton beam direction. The pseudorapidity η is defined as $-\ln[\tan(\theta/2)]$. The transverse momentum of a particle is $p_T = p \sin \theta$, where p is the momentum measured in the spectrometer. The analogous quantity using calorimeter energies is called the transverse energy E_T . The difference between the vector sum of all the transverse energies and zero is the missing transverse energy \cancel{E}_T .
- [7] F. Abe *et al.*, Phys. Rev. D **45**, 1448 (1992).
- [8] C. Balázs, J. L. Diaz-Cruz, H.-J. He, T. Tait, and C.-Y. Yuan, Phys. Rev. D **59**:055016 (1999); M. Carena, S. Mrenna, C.E.M. Wagner, Phys. Rev.D **60**:075010 (1999).
- [9] T. Sjöstrand, Comput. Phys. Commun. **82**, 74 (1994).
- [10] F. Abe *et al.*, Phys. Rev. Lett. **74**, 2626 (1995).
- [11] G. Marchesini *et al.*, Comput. Phys. Commun. **67**, 465 (1992).
- [12] F. Ptohos (for the CDF collaboration), proceedings of the International Europhysics Conference on High Energy Physics 99, Tampere, Finland, July 17, 1999.
- [13] F. Abe *et al.*, Phys. Rev. Lett. **79**, 1992 (1997).
- [14] G. Zech, Nucl. Instrum. Methods Phys. Res., Sect A**277**, 608 (1989). This formula also admits a Bayesian interpretation, see O. Helene, Nucl. Instrum. Methods, **212**, 319 (1983). See also the discussion of eq. (7) in B. P. Roe and M. B. Woodrooffe, Phys. Rev. **D60** 053009 (1999).
- [15] See for instance R. Cousins and V. Highland, Nucl. Instrum. Methods Phys. Res., Sect A**320**, 331 (1992). We use numerical techniques to solve the general case.

[16] The LEP working group for Higgs boson searches. CERN-EP/2000-055; ALEPH 2000-028 CONF 2000-023; DELPHI 2000-050 CONF 365; L3 note 2525; OPAL TN646, March 15, 2000.

TABLES

TABLE I. Number of observed and expected background events after the final selection and for the different SM contributions as a function of mass. Last three columns show the total acceptances and expected 95% C.L. upper limits on the number of signal events (N_{signal}) and on $\sigma \times \mathcal{BR}$, respectively.

m_φ (GeV/c ²)	Observed Events	Expected Background	Acceptance (%)	N_{signal} (95% C.L.)	$\sigma \times \mathcal{BR}$ (pb, 95% C.L.)
70	5	4.6 ± 1.4	0.16 ± 0.03	7.9	53.3
80	4	4.6 ± 1.4	0.22 ± 0.04	6.6	31.7
90	3	3.8 ± 1.3	0.23 ± 0.04	5.8	27.1
100	3	3.8 ± 1.3	0.25 ± 0.04	5.9	25.7
110	2	3.7 ± 1.1	0.25 ± 0.04	4.8	20.7
120	2	3.5 ± 1.1	0.28 ± 0.05	4.9	19.2
130	1	2.6 ± 0.9	0.28 ± 0.05	4.1	15.8
140	1	1.7 ± 0.8	0.29 ± 0.05	4.3	16.2
150	0	1.5 ± 0.8	0.30 ± 0.05	3.2	11.5
200	0	1.2 ± 0.7	0.41 ± 0.07	3.2	8.5
250	0	1.0 ± 0.7	0.47 ± 0.08	3.2	7.5
300	0	0.1 ± 0.4	0.59 ± 0.09	3.2	5.8

TABLE II. Expected QCD, fake triple tags, $t\bar{t}$, $Wb\bar{b} + Wc\bar{c}$, $Zb\bar{b} + Zc\bar{c}$, and total number of background events as a function of mass.

m_φ (GeV/c ²)	QCD	Fakes	$t\bar{t}$	$Wb\bar{b} + Wc\bar{c}$	$Zb\bar{b} + Zc\bar{c}$	Total
70	2.97 ± 0.70	0.5 ± 1.2	0.70 ± 0.18	0.09 ± 0.06	0.37 ± 0.02	4.6 ± 1.4
80	2.97 ± 0.70	0.5 ± 1.2	0.70 ± 0.18	0.09 ± 0.06	0.37 ± 0.02	4.6 ± 1.4
90	2.16 ± 0.55	0.5 ± 1.2	0.70 ± 0.18	0.09 ± 0.06	0.37 ± 0.02	3.8 ± 1.3
100	2.16 ± 0.55	0.5 ± 1.2	0.70 ± 0.18	0.09 ± 0.07	0.37 ± 0.02	3.8 ± 1.3
110	2.16 ± 0.55	0.4 ± 0.9	0.68 ± 0.18	0.09 ± 0.07	0.37 ± 0.02	3.7 ± 1.1
120	2.16 ± 0.55	0.3 ± 0.9	0.66 ± 0.17	0.07 ± 0.06	0.29 ± 0.02	3.5 ± 1.1
130	1.44 ± 0.45	0.3 ± 0.8	0.64 ± 0.17	0.05 ± 0.05	0.21 ± 0.02	2.6 ± 0.9
140	0.73 ± 0.40	0.2 ± 0.7	0.60 ± 0.16	0.04 ± 0.05	0.16 ± 0.02	1.7 ± 0.8
150	0.73 ± 0.40	0.1 ± 0.7	0.55 ± 0.15	0.03 ± 0.05	0.12 ± 0.02	1.5 ± 0.8
200	0.73 ± 0.40	0.1 ± 0.6	0.32 ± 0.09	0.00 ± 0.00	0.00 ± 0.00	1.2 ± 0.7
250	0.73 ± 0.40	0.1 ± 0.6	0.17 ± 0.05	0.00 ± 0.00	0.00 ± 0.00	1.0 ± 0.7
300	0.01 ± 0.01	0.1 ± 0.4	0.00 ± 0.00	0.00 ± 0.00	0.00 ± 0.00	0.1 ± 0.4

FIGURES

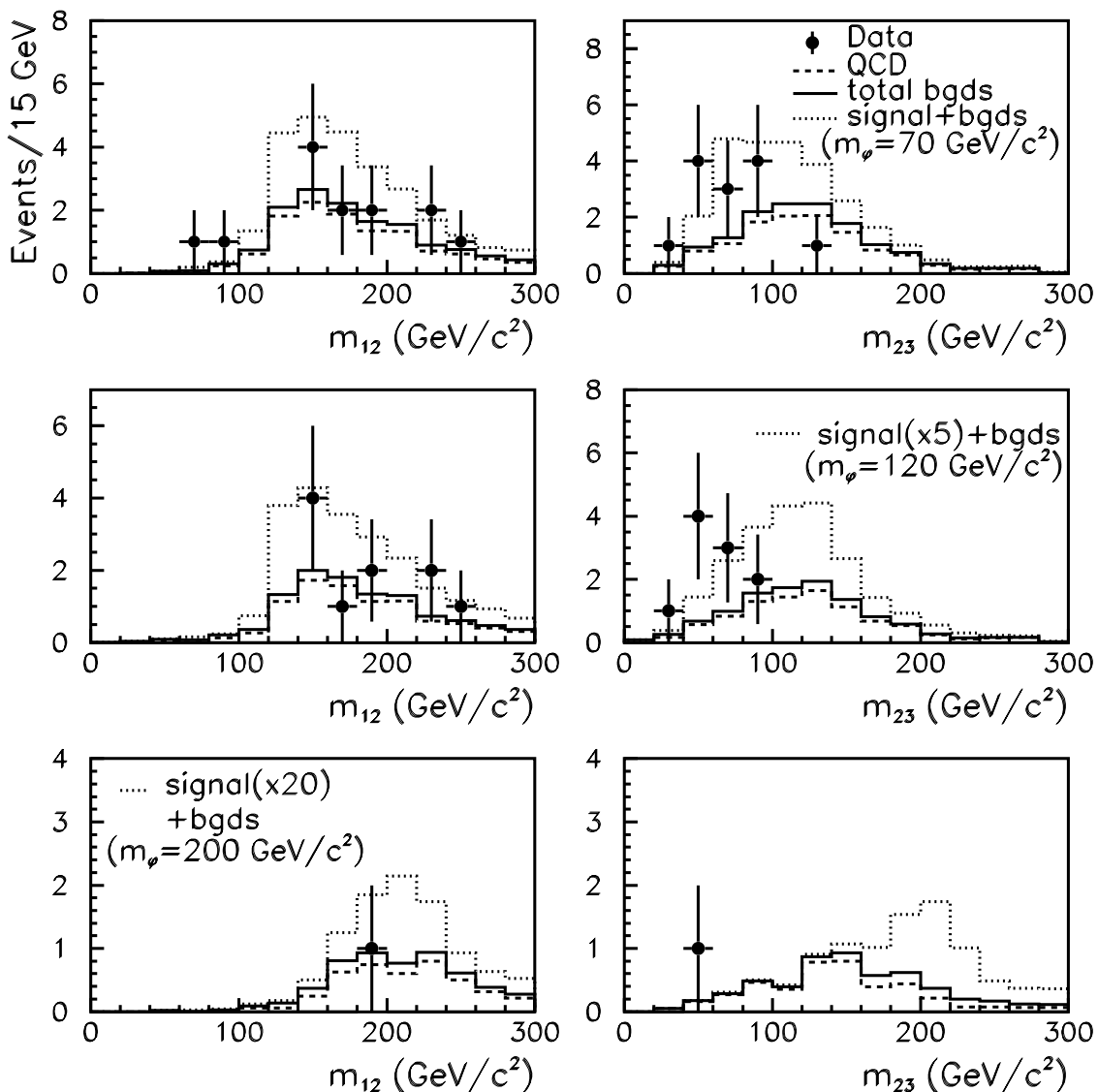


FIG. 1. Invariant mass distributions m_{12} and m_{23} for the observed triple b -tagged sample corresponding to the $m_\phi = 70 \text{ GeV}/c^2$ (top), $m_\phi = 120 \text{ GeV}/c^2$ (middle), and $m_\phi = 200 \text{ GeV}/c^2$ (bottom) selections. The data is compared to the expected QCD only background, the total SM backgrounds, and the total background plus signal for $\tan\beta = 50$ and the *no mixing* case. The use of m_{23} for $m_\phi \leq 120 \text{ GeV}/c^2$, and m_{12} for $m_\phi > 120 \text{ GeV}/c^2$ maximizes the fraction of correct jet assignments and enhance the signal resolution (see text). The mass cuts are not applied.

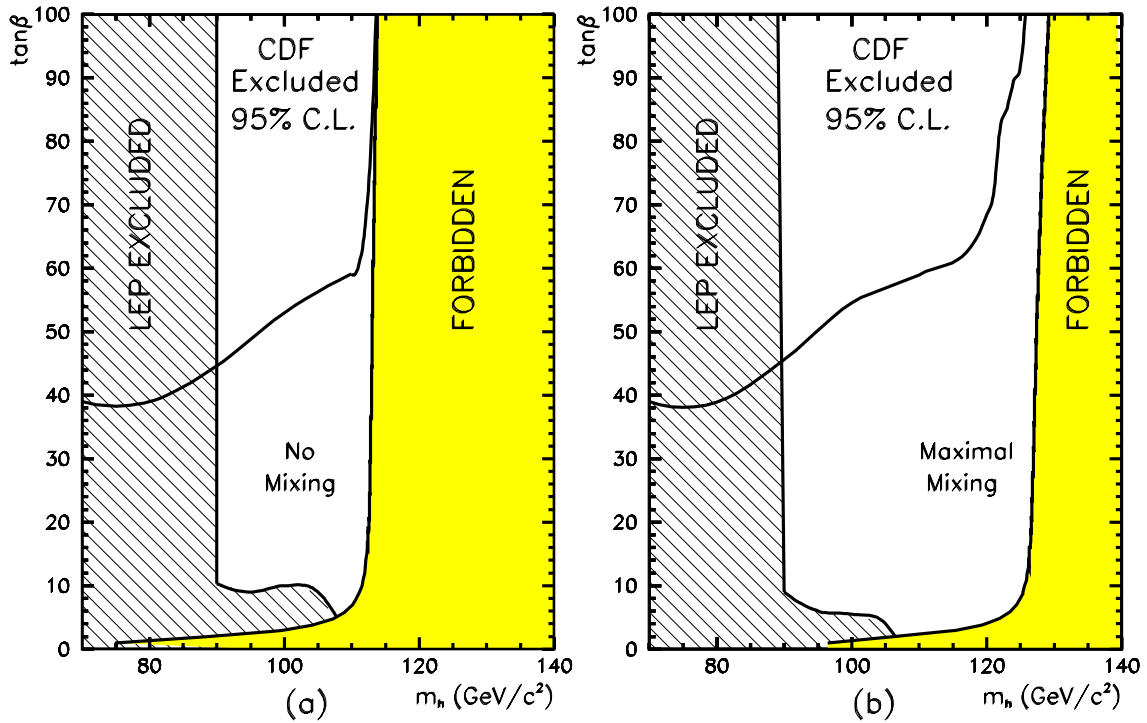


FIG. 2. CDF 95% C.L. excluded region in the parameter space $m_h - \tan \beta$ for the two stop mixing scenarios: (a) *no mixing*, and (b) *maximal mixing*. Also shown are the theoretically forbidden regions and the LEP exclusion region for their *no mixing* and m_h^{max} scenarios [16].

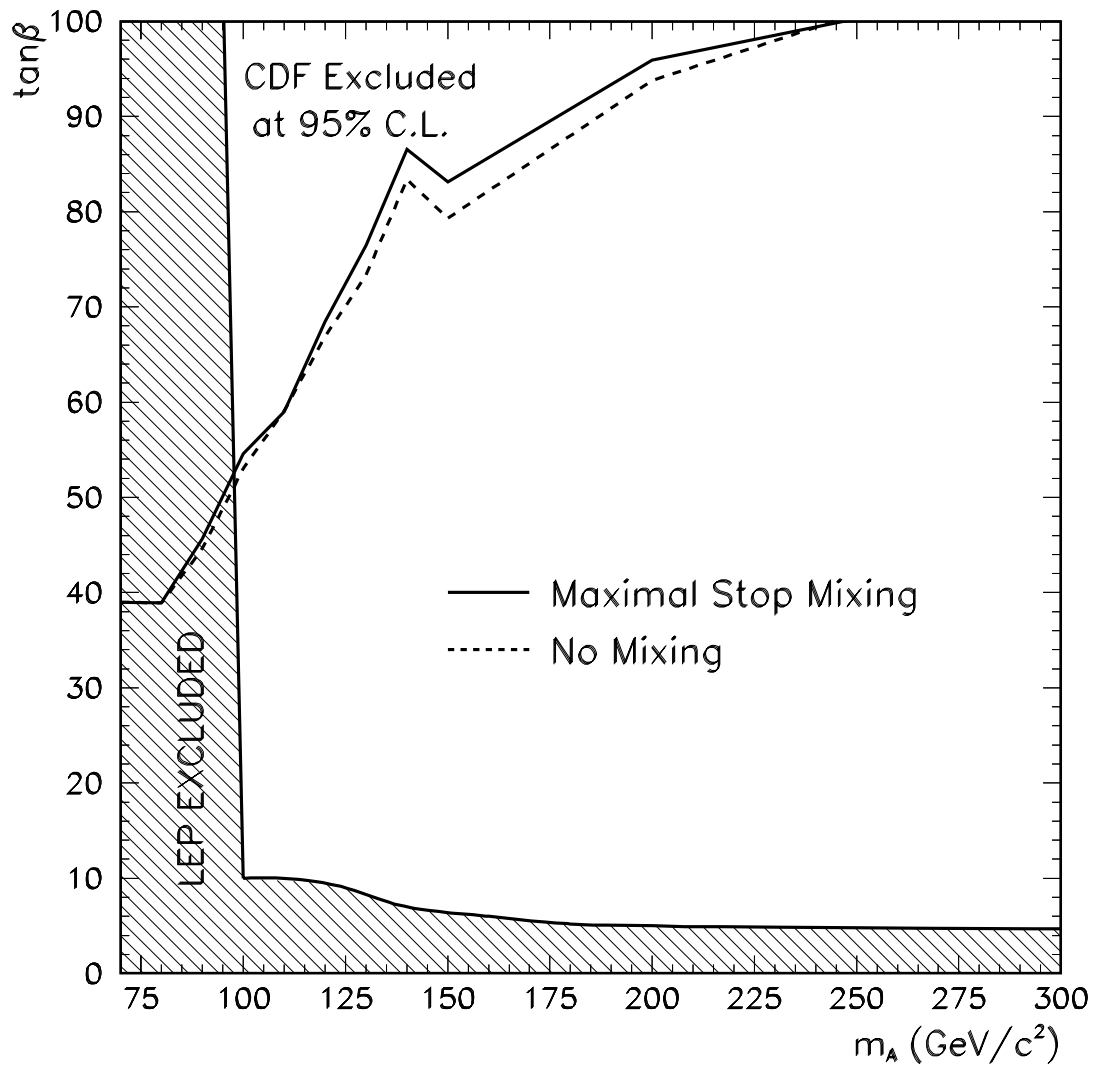


FIG. 3. CDF 95% C.L. excluded region in the parameter space $m_A - \tan\beta$ for the two stop mixing scenarios: *no mixing* (dashed lines) and *maximal mixing* (solid line). Also shown is the LEP exclusion region for the *no mixing* scenario [16].